



Effect of elements with positive enthalpy of mixing on mechanical properties of bulk metallic glasses

S. Schmitz*, W. Löser, H. Klauß, B. Büchner

IFW Dresden, P.O. Box 270116, D-01171 Dresden, Germany

ARTICLE INFO

Article history:

Received 2 July 2010

Received in revised form 1 December 2010

Accepted 8 December 2010

Available online 15 December 2010

Keywords:

Metallic glasses

Rapid solidification

Mechanical properties

ABSTRACT

Samples of $(\text{Cu}_{46}\text{Zr}_{46}\text{Al}_8)_{100-x}\text{Z}_x$ metallic glass forming alloys with diameters 2–6 mm were prepared by injection casting. The effect of minor amounts of elements $Z = \text{Gd}, \text{Co}$ and Re with positive enthalpy of mixing within the Gd-Zr , Cu-Co and Cu-Re terminal systems was compared. The addition of Gd up to $x = 2$ slightly enhances the glass forming ability, Co reduces the critical diameter of bulk metallic glass formation, whereas even for small fractions of Re bulk samples were crystalline, but only amorphous splats can be prepared. Both Gd and Co diminish the crystallization temperature T_x with respect to the $\text{Cu}_{46}\text{Zr}_{46}\text{Al}_8$ master alloy, but in Re -bearing splats T_x is increased. Alloying with optimum amounts of Gd and Co up to $x = 2$ leads to plastic deformability of rods, 2 and 3 mm in diameter, in comparison with the brittle $\text{Cu}_{46}\text{Zr}_{46}\text{Al}_8$ bulk metallic glass.

© 2010 Elsevier B.V. All rights reserved.

1. Introduction

Normally, large negative heats of mixing among the constituent elements of alloys provide a favourable condition for bulk metallic glass (BMG) formation [1]. Phase separation in the liquid state, experimentally observed if repulsive interactions are present between two major constituent elements, can lead to the formation of phase separated metallic glasses [2–5]. It has been shown that the BMGs can exhibit enhanced plasticity as well as glass forming ability (GFA) if a minor amount of a constituent element with positive heat of mixing is added [5–11]. The degree of local heterogeneity in the glassy matrix, depending on the atomic species added, its fraction and the cooling rate during solidification, may affect the room-temperature properties of BMGs. In particular, it was shown that for the BMG forming alloy Cu-Zr-Al the plasticity can be improved by the addition of minor amounts of Y and Gd possessing positive enthalpies of mixing with Zr . Here, we study the effect of minor additions of the elements $Z = \text{Gd}, \text{Co}$ and Re on GFA, microstructure of cast samples and deformation behavior of a $\text{Cu}_{46}\text{Zr}_{46}\text{Al}_8$ master alloy with well-known superior GFA. The three elements exhibit positive enthalpies of mixing within different binary terminal systems, Gd-Zr , Cu-Co and Cu-Re , which give rise to metastable liquid miscibility gaps for Cu-Co [12] and Gd-Zr [13], but a stable liquid miscibility gap at elevated temperature for Cu-Re [14]. One special aim of the work is to elucidate the effect of various amounts of these elements, which exhibit quite different features of immiscibility regarding the main constituents of the

Cu-Zr-Al glass-forming alloy, concomitant with the variation of the cooling rate by casting specimens with different diameters [15].

2. Experimental

The multi-component $(\text{Cu}_{46}\text{Zr}_{46}\text{Al}_8)_{100-x}\text{Z}_x$ ($x = 1-4$) alloys were prepared from elements of 99.99 wt.% purity, $\text{Zr}, \text{Cu}, \text{Al}$, and $Z = \text{Co}, \text{Gd}, \text{Re}$, by arc melting under a purified Zr -gettered argon atmosphere on a water-cooled Cu hearth. The buttons were remelted in a Hukin-type cold-crucible radio frequency induction furnace under Ar atmosphere and cast into Cu -molds to form bulk rods 6 mm in diameter and 75 mm in length. Rods with 2 and 3 mm diameter were prepared by injection casting in Cu -molds. In addition, thin foils with thicknesses $\sim 40 \mu\text{m}$ were produced in a splat quenching apparatus.

Structural investigations were carried out by X-ray diffraction (XRD) with $\text{Cu K}\alpha$ radiation using a Rigaku diffractometer. For microstructure and phase identification, sample cross sections were examined by using a Zeiss Jenapol optical microscope and by scanning electron microscopy (SEM) in the backscattered electron (BSE) and secondary electron (SE) mode using a Philips XL30 device. The composition of the phases was measured by electron probe X-ray microanalysis (EPMA) in the energy dispersive mode (EDS). A TECNAI T20 transmission electron microscope (TEM) with a LaB_6 cathode operated at 200 kV accelerating voltage coupled with energy-dispersive X-ray analysis (EDX) was used for local structure analysis. Differential scanning calorimeter (DSC) studies of samples were accomplished up to 650°C in an argon atmosphere using a Netzsch DSC 404 device at a heating rate of 20 K/min.

Compression tests were performed with an Instron 8562 electromechanical testing device under quasistatic loading (strain rate: 7×10^{-5} to $1 \times 10^{-4} \text{ s}^{-1}$) at room temperature. The cylindrical test samples with a diameter to length ratio 1:2 were cut from as-cast rods.

3. Results

3.1. Structure and thermal stability

Similar to the $\text{Cu}_{46}\text{Zr}_{46}\text{Al}_8$ basic composition $(\text{Cu}_{46}\text{Zr}_{46}\text{Al}_8)_{100-x}\text{Z}_x$ are bulk metallic glass forming alloys

* Corresponding author. Tel.: +49 351 4659 762; fax: +49 351 4659 313.

E-mail address: s.schmitz@ifw-dresden.de (S. Schmitz).

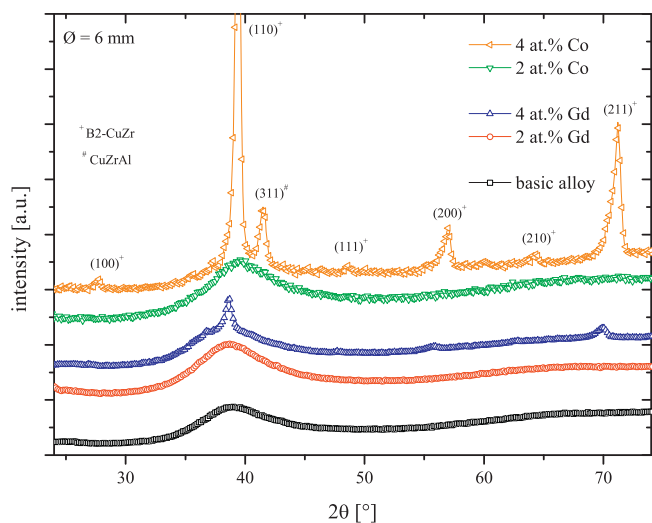


Fig. 1. The X-ray diffraction pattern of as-cast rods 6 mm in diameter of $(\text{Cu}_{46}\text{Zr}_{46}\text{Al}_8)_{100-x}\text{Z}_x$ alloys containing the element fractions $Z = \text{Co}$ or Gd with $x = 0$ (basic alloy), 2 and 4 at.%. The principal reflections of the crystalline B2-CuZr and a CuZrAl structure type phase, respectively, are denoted.

for $Z = \text{Co}$ and Gd . The X-ray diffraction patterns, Fig. 1, show that as-cast rods 6 mm in diameter exhibit an amorphous structure if the fraction of Co or Gd does not exceed $x = 2$, however small crystalline fractions cannot be excluded by X-ray diffraction.

The $(\text{Cu}_{46}\text{Zr}_{46}\text{Al}_8)_{96}\text{Gd}_4$ and $(\text{Cu}_{46}\text{Zr}_{46}\text{Al}_8)_{96}\text{Co}_4$ samples display crystalline reflections of the B2-CuZr and the CuZrAl cubic structure type, respectively. For these two alloys bulk amorphous rods were only obtained up to 3 mm diameter. According to the HRTEM images shown in Fig. 2, the Co-bearing alloy normally shows a homogeneous amorphous structure which is proven by the halo in the selected area diffraction (SAD) pattern (Fig. 2a). However, small areas with crystalline structure are embedded in the glassy matrix, which also lead to additional reflections in the SAD pattern (Fig. 2b). The crystalline fraction detected in the samples is eventually triggered by chemical heterogeneities.

For Re-containing alloys $(\text{Cu}_{46}\text{Zr}_{46}\text{Al}_8)_{100-x}\text{Re}_x$ ($x = 1, 2$) no bulk amorphous samples have been received even for rods 2 mm in diameter. As shown by the SEM image, Fig. 2c, they form small Re-rich precipitates, which initiate the complete crystallization of B2-CuZr and CuZrAl type phases. Only thin $(\text{Cu}_{46}\text{Zr}_{46}\text{Al}_8)_{99}\text{Re}_1$ splats of 40 μm thickness display a diffraction pattern without crystalline reflections.

The effect of the element Co on the thermal stability of bulk amorphous $(\text{Cu}_{46}\text{Zr}_{46}\text{Al}_8)_{100-x}\text{Co}_x$ samples ($\varnothing = 3$ mm) on isochronal heating with 20 K/min is demonstrated in Fig. 3. The slight endothermic upturn of the DSC signal with an inflection point is defined as the glass transition temperature $T_g = 430$ °C. The strong exothermic peaks with the onset temperatures at $T_x = 500$ °C ($x = 1$), 495 °C ($x = 2$), and 490 °C ($x = 4$) are attributed to the crystallization of the amorphous matrix. The glass transition temperature T_g is not much affected by small Co additions but the crystallization temperature T_x is slightly reduced signaling the poorer GFA. The enthalpy of crystallization drops from 39 J/g ($x = 1$) to 18 J/g ($x = 2$).

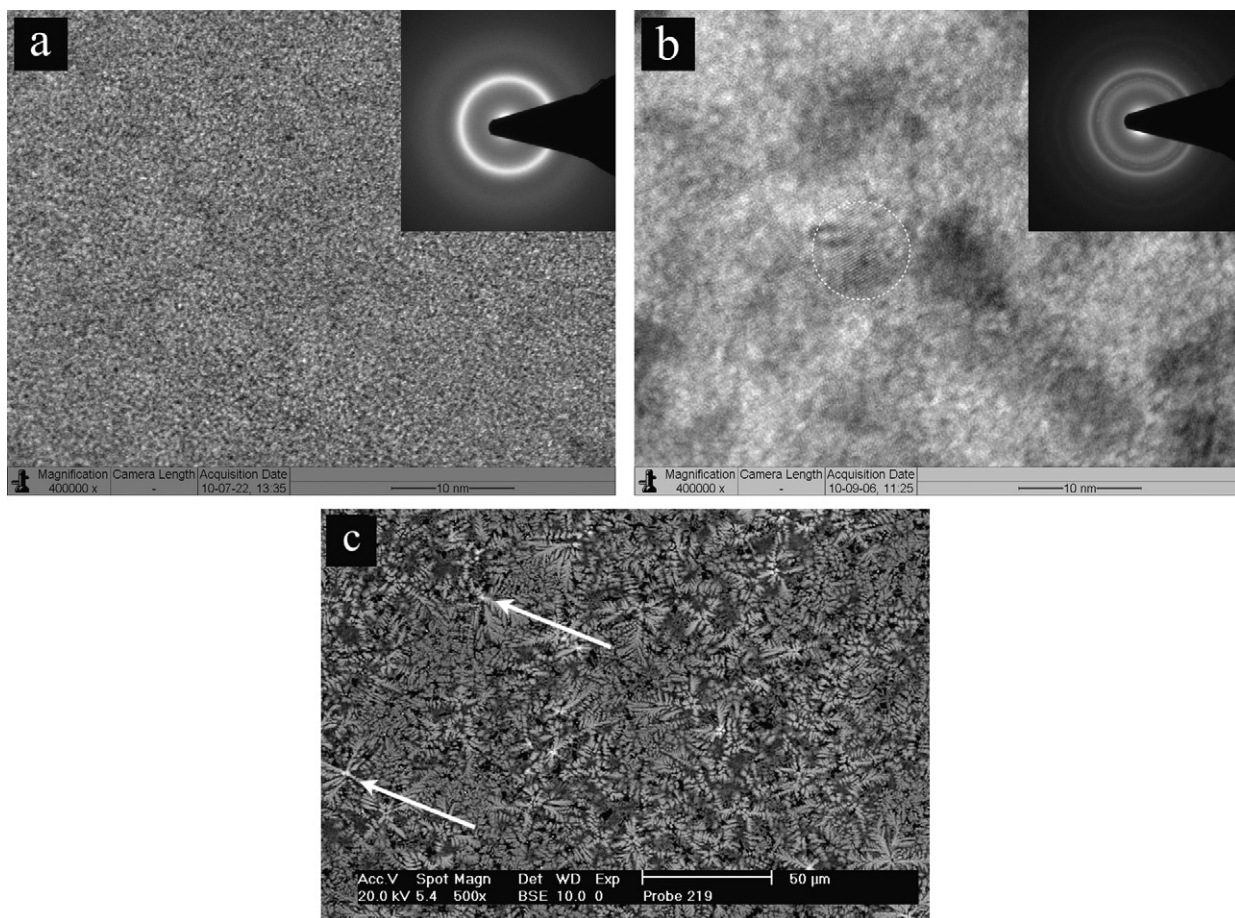


Fig. 2. TEM images and SAD patterns (insets) of a $(\text{Cu}_{46}\text{Zr}_{46}\text{Al}_8)_{99}\text{Co}_1$ rod 3 mm in diameter. (a) Amorphous region and (b) amorphous region with an embedded nanocrystallite. The dashed circle indicates the nanocrystallite. (c) SEM backscattered electron image of a crystalline $(\text{Cu}_{46}\text{Zr}_{46}\text{Al}_8)_{98}\text{Re}_2$ rod 3 mm in diameter. The arrows point to Re-rich precipitates.

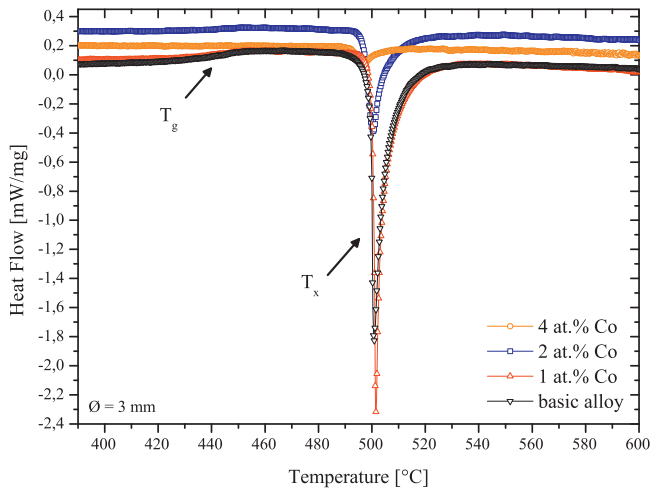


Fig. 3. DSC scans of $(\text{Cu}_{46}\text{Zr}_{46}\text{Al}_8)_{100-x}\text{Co}_x$ amorphous alloys from rods 3 mm in diameter at heating rates 20 K/min.

and 2.6 J/g for ($x=4$). This is not only because of the change in the glassy structure by adding the element with positive enthalpy of mixing, but also largely due to the appreciable crystalline fractions for the higher Co content ($x \geq 2$). Addition of Gd also reduced $T_x = 495^\circ\text{C}$ for $(\text{Cu}_{46}\text{Zr}_{46}\text{Al}_8)_{99}\text{Gd}_1$ compared with $T_x = 500^\circ\text{C}$ of the basic alloy and to $T_x = 475^\circ\text{C}$ for $(\text{Cu}_{46}\text{Zr}_{46}\text{Al}_8)_{96}\text{Gd}_4$ which confirms similar tendencies reported for melt spun ribbons [11]. However, the enthalpy of crystallization decreases less strong, from 46 J/g ($x=1$) to 31 J/g ($x=4$), than for Co additions, pointing to the better GFA [16] and a smaller crystalline fraction of the Gd-bearing alloys.

3.2. Mechanical properties and fracture mode

Room temperature compressive stress–strain curves of as-cast $(\text{Cu}_{46}\text{Zr}_{46}\text{Al}_8)_{100-x}\text{Co}_x$ samples with 2 and 3 mm in diameter are shown in Fig. 4. The initial BMG $\text{Cu}_{46}\text{Zr}_{46}\text{Al}_8$ exhibits high strength of 1700–1800 MPa and appreciable elastic elongation up to $\varepsilon = 1.8\%$, but does not display any substantial plastic deformation. The slight leveling-off of the stress–strain curves of 2 mm diameter samples at high stresses (~ 1800 MPa) suggests some plastic deformation, but the serrated flow may be due to inhomogeneous deformation in shear bands accompanied by micro-cracking. Samples of the basic alloy with larger diameter fail upon yield and do not show any plasticity. Small amounts of Co ($x=1$) only lead to a minor improvement of the compressive deformation behavior of samples 3 mm in diameter, which show about $\varepsilon_p \approx 1\%$ plastic elongation (Fig. 4b).

If the Co fraction is increased to $x=2$ the plastic deformation is further improved and the plastic elongation can reach $\varepsilon_p \approx 2\%$ and a strain to fracture up to $\varepsilon_f \approx 4\%$ for samples with 2 mm in diameter. The elastic module of $E = 100 \pm 5$ GPa and the yield stress $\sigma_y = 1800$ MPa remain virtually unchanged by the Co addition. With increasing diameter the compressive deformation behavior is obviously changed and the sizeable plastic deformation is accompanied by reduction of the yield stress, which is in the range between $\sigma_y = 800$ and 1600 MPa for specimen 3 mm in diameter, and apparent work hardening. We attribute the improved plastic deformation to the higher crystalline fraction caused by the reduced cooling rate (cf. Figs. 1 and 2b). For $x=4$ the optimum Co portion is exceeded for both sample sizes, which leads both to a less significant plastic deformation $\varepsilon_p \leq 1\%$ and a reduction of the yield stress of the specimens. The apparent scatter of stress–strain curves for the same concentration and sample size may be caused by cooling rate fluctuations in the casting

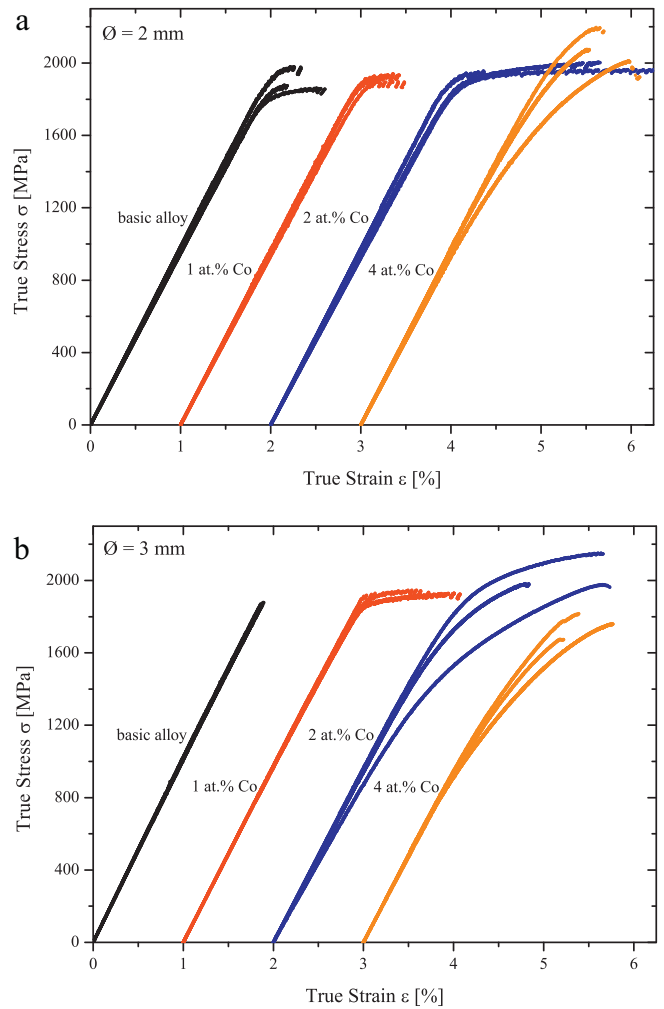


Fig. 4. Room temperature compressive stress–strain curves of $(\text{Cu}_{46}\text{Zr}_{46}\text{Al}_8)_{100-x}\text{Co}_x$ of injection cast rods with diameters (a) $\varnothing = 2$ mm and (b) $\varnothing = 3$ mm.

process, which induces local structure variation in the as-cast rods.

The Gd containing alloys $(\text{Cu}_{46}\text{Zr}_{46}\text{Al}_8)_{100-x}\text{Gd}_x$ displayed an improved plastic deformation up to $\varepsilon_p \approx 2.5\%$ and $\varepsilon_f \geq 4\%$ only for $x=2$ for samples 3 mm in diameter. The yield stress reduction by Gd to 1700–1500 MPa is much less significant than for Co-bearing samples. Specimens with $x=4$ do not show plastic deformability. The observed improvement of the deformation behavior and the optimum Gd fraction $x=2$ are similar to previously reported $\text{Cu}_{46}\text{Zr}_{47-x}\text{Al}_7\text{Gd}_x$ rods with 1 and 2 mm diameter [11].

The stress–strain curves of Re-bearing samples $(\text{Cu}_{46}\text{Zr}_{46}\text{Al}_8)_{100-x}\text{Re}_x$ must be distinguished from the above-discussed behavior. They display a high degree of plastic deformation up to $\varepsilon_p \approx 4.5\%$, high ultimate stress $\sigma_{\text{max}} = 1600$ MPa, but rather low yield stresses of $\sigma_y = 400$ –800 MPa and extended strain hardening. Therefore, the mechanical properties rather resemble those of their constituent crystalline phases, basically the B2-CuZr type phase, which is ductile but exhibits a comparatively low yield strength $\sigma_y \approx 450$ –490 MPa [17], and will not be discussed in detail.

Fracture surfaces reflect the different mechanical behavior of the samples in compression testing. The SEM image of the $\text{Cu}_{46}\text{Zr}_{46}\text{Al}_8$ BMG displays a typical vein pattern (Fig. 5a), indicating that the sample has experienced thermal softening and large deformation.

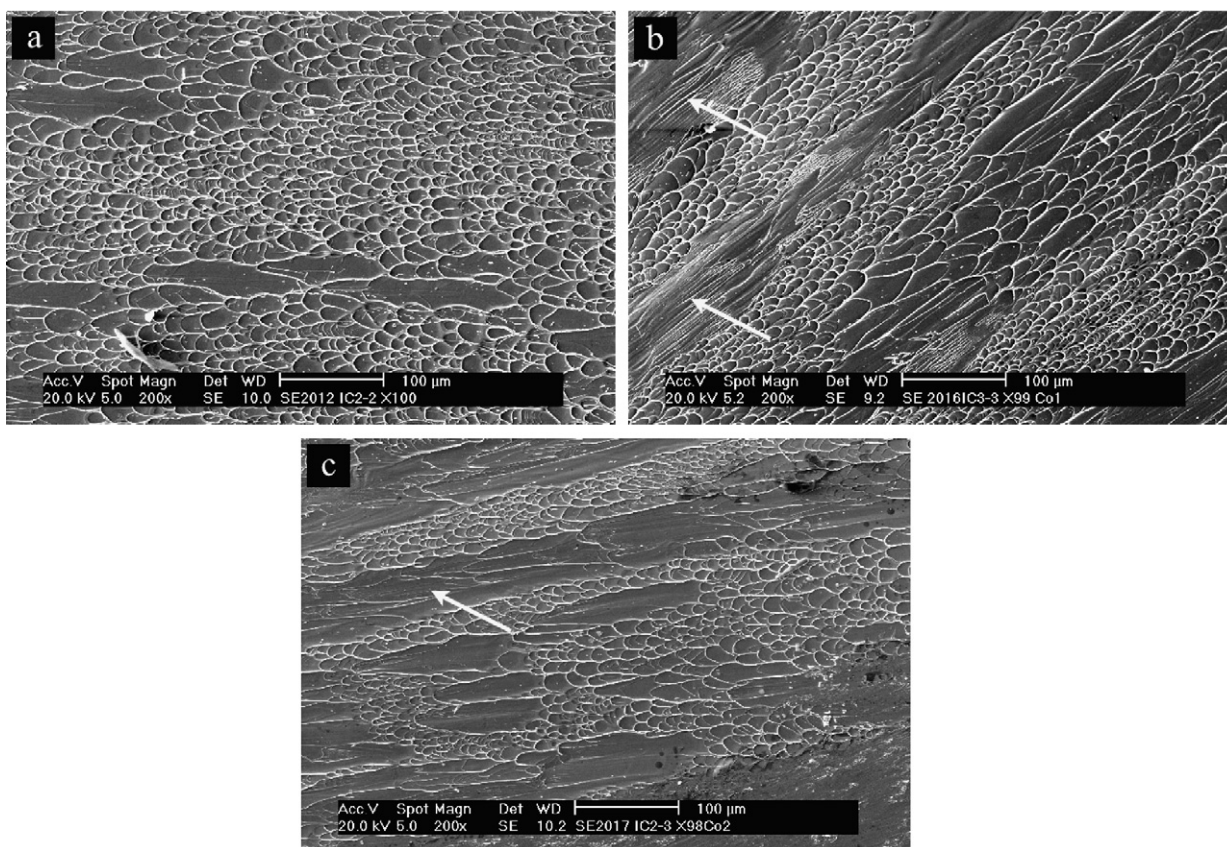


Fig. 5. SEM secondary electron images of fracture surfaces after compressive testing. (a) $\text{Cu}_{46}\text{Zr}_{46}\text{Al}_8$ BMG specimen ($\varnothing = 2$ mm), (b) $(\text{Cu}_{46}\text{Zr}_{46}\text{Al}_8)_{99}\text{Co}_1$ BMG specimen ($\varnothing = 3$ mm), and (c) $(\text{Cu}_{46}\text{Zr}_{46}\text{Al}_8)_{98}\text{Co}_2$ BMG specimen ($\varnothing = 2$ mm). The arrows point to surface ripples indicating ductile deformation.

On contrary, the fracture surface of $(\text{Cu}_{46}\text{Zr}_{46}\text{Al}_8)_{99}\text{Co}_1$ is characterized by elongated areas with alternating coarse and fine vein patterns. The coarse regions exhibit some smooth surface ripples, signaling plastic deformation. For the $(\text{Cu}_{46}\text{Zr}_{46}\text{Al}_8)_{98}\text{Co}_2$ specimens alternating areas with completely smooth appearance and with vein pattern, respectively, are detected, which spread along the fracture surface forming an angle of $\sim 45^\circ$ with the sample axis.

4. Discussion and conclusions

Randomly distributed chemical heterogeneities in the amorphous matrix, caused by additions of elements with positive enthalpies of mixing, are considered as a prospective concept for improving the ductility of BMG's. This has been proven for $\text{Cu}_{46}\text{Zr}_{47-x}\text{Y}_x\text{Al}_7$ [5] and $\text{Cu}_{46}\text{Zr}_{47-x}\text{Gd}_x\text{Al}_7$ [11] where some plastic deformation was achieved for small samples ($\varnothing = 1\text{--}2$ mm) in a limited concentration range of the elements with positive enthalpy of mixing, Y and Gd. For the latter system the beneficial effects on the mechanical properties are principally confirmed in the present work for a similar composition and for somewhat larger rod diameters although an alternative origin of this effect, the capability of Gd to remove oxygen from the glassy matrix is discussed. It may not only increase the GFA [16] but also improve the mechanical properties. Compressive stress–strain curves of our $(\text{Cu}_{46}\text{Zr}_{46}\text{Al}_8)_{100-x}\text{Co}_x$ samples, shown in Fig. 4, reveal that alloying with Co has a more distinct effect on the plastic deformability than Gd. Oxygen gettering in the glassy matrix can be excluded for Co. Therefore, we can indeed assume that chemical heterogeneities enhance the strength of the amorphous matrix, which leads to a higher resistance against thermal softening within local shear bands. However, nanocryst-

alline regions embedded in the glassy matrix, which are eventually triggered by chemical heterogeneities, may also contribute to the improved deformability.

The elongated areas with coarsened or no shear band patterns on the fracture surface of Co containing samples support this assumption. Similar to the previously studied systems, the biggest enhancement of plastic elongation was achieved for the optimum Co content $x=2$. If this limit is exceeded ($x=4$) appreciable fractions of crystalline phases are formed within the glassy matrix, which are verified in the X-ray diffraction pattern and by the drastically reduced enthalpy of crystallization of the samples. However, for $(\text{Cu}_{46}\text{Zr}_{46}\text{Al}_8)_{98}\text{Co}_2$ the difference between samples prepared with different cooling rates is also apparent. In particular, for samples with larger diameter ($\varnothing = 3$ mm) the enhanced plastic deformation is accompanied by a sizeable decrease of the yield strength. It was discovered only recently that crystalline (B2–CuZr) heterogeneities can also enhance the plasticity of Cu–Zr(–Al) based BMG samples but they cause the yield strength to drop [16,17]. In the $(\text{Cu}_{46}\text{Zr}_{46}\text{Al}_8)_{100-x}\text{Co}_x$ system we observed a drop in the yield strength not only for the samples prepared with a lower cooling rate but also for samples with higher Co fractions ($x=4$), which definitely contain some crystalline volume fraction. Therefore, the strengthening of the glassy matrix by nano-heterogeneities may be superimposed by the effects of small crystalline (B2 CuZr-type) phase precipitates, which also can improve the plasticity [16–18].

The concept of improved mechanical properties for BMG systems, by addition of small amounts of elements with positive enthalpy of mixing is of huge interest for developing new alloy designs. It may involve alternative structure effects, which warrant further studies with sophisticated methods of structure analysis.

Acknowledgment

The authors thank Ch. Mickel for additional TEM investigations, S. Müller-Litvanyi and S. Pichl for technical assistance and simulating discussions. S. Schmitz is grateful for the financial support provided by the “Pakt für Forschung Programm” for his stay at the IFW Dresden.

References

- [1] A. Inoue, *Acta Mater.* 48 (2000) 279–306.
- [2] A.A. Kündig, M. Ohnuma, D.H. Ping, T. Ohkubo, K. Hono, *Acta Mater.* 52 (2004) 2441–2448.
- [3] B.J. Park, H.J. Chang, D.H. Kim, W.T. Kim, *Appl. Phys. Lett.* 85 (2004) 6353–6355.
- [4] N. Mattern, U. Kühn, A. Gebert, T. Gemming, M. Zinkevich, H. Wendrock, L. Schultz, *Scripta Mater.* 53 (2005) 271–274.
- [5] E.S. Park, D.H. Kim, *Acta Mater.* 54 (2006) 2597–2604.
- [6] L.-Q. Xing, Y. Li, K.T. Ramesh, J. Li, T.C. Hufnagel, *Phys. Rev. B* 64 (2001) 180201.
- [7] E.S. Park, J.Y. Lee, D.H. Kim, *J. Mater. Res.* 20 (2005) 2379–2385.
- [8] M.H. Lee, D.H. Bae, W.T. Kim, D.H. Kim, *Mater. Trans.* 44 (2003) 2084–2087.
- [9] E.S. Park, D.H. Kim, T. Ohkubo, K. Hono, *J. Non-Cryst. Solids* 351 (2005) 1232–1238.
- [10] J.C. Oh, T. Ohkubo, Y.C. Kim, E. Fleury, K. Hono, *Scripta Mater.* 53 (2005) 165–169.
- [11] E.S. Park, J.S. Kyeong, D.H. Kim, *Scripta Mater.* 57 (2007) 49–52.
- [12] Y. Nakagawa, *Acta Metall.* 6 (1958) 704–711.
- [13] S. Schmitz, H.-G. Lindenkreuz, N. Mattern, W. Löser, B. Büchner, *Intermetallics* 18 (2010) 1941–1945.
- [14] P.R. Subramanian, D.E. Laughlin, in: T.B. Massalski (Ed.), *Binary Alloy Phase Diagrams*, 2nd ed., ASM International, Materials Park (OH), 1990, pp. 1464–1465.
- [15] W. Löser, J. Das, A. Güth, H.-J. Klauß, C. Mickel, U. Kühn, J. Eckert, S.K. Roy, L. Schultz, *Intermetallics* 12 (2004) 1153–1158.
- [16] H.M. Fu, H. Wang, H.F. Zhang, Z.Q. Hu, *Scripta Mater.* 55 (2006) 147–150.
- [17] S. Pauly, G. Liu, G. Wang, U. Kühn, N. Mattern, J. Eckert, *Acta Mater.* 57 (2009) 5445–5453.
- [18] S. Pauly, S. Gorantla, G. Wang, U. Kühn, J. Eckert, *Nat. Mater.* 9 (2010) 473–477.